Effect of Metallurgical Parameters on Shear Band Formation in Low-Carbon (~0.20 Wt Pct) Steels*

MARC A. MEYERS and CRAIG L. WITTMAN

With the objective of establishing the effects of the metallurgical condition on the propensity to form adiabatic shear bands, low-carbon steels (AISI 1018 and 8620) having widely different temperability responses were subjected to impact by cylindrical projectiles in the velocity range of 450 to 1050 m/s. These steels received a variety of mechanical and thermal treatments that provided a wide range of microstructures and mechanical responses. The propensity for shear band formation was strongly dependent on the mechanical response. It was measured by counting the length of shear bands per cross section. Microstructural characterization of the bands revealed that white-etching bands were only observed in the quenched and quenched-and-tempered conditions.

I. INTRODUCTION

WHEN the rate of work softening due to temperature increase exceeds the rate of work hardening and strain-rate hardening in a material undergoing deformation, plastic strain might concentrate into narrow regions, loosely termed "adiabatic shear bands."[1-5] The term adiabatic is used because only a small amount of the heat generated by the deformation process is considered to be transferred to the surrounding area during the ongoing deformation. While shear bands have been observed in low strain-rate deformation, the term "adiabatic shear bands" is reserved for materials deformed at high strain rates ($\dot{\gamma} > 10^2\ s^{-1}$).

Failure of materials by adiabatic shear occurs in machining, punching, forging, high-velocity deformation, and ballistic impact. This last application is of great importance, since it is known that adiabatic shear is a precursor to armor and projectile failure. Shear bands have been reported in copper, brass, aluminum alloys, titanium and its alloys, magnesium, plastics, and most commonly, in steels.[1] The thickness of such bands varies from 0.1 to 100 μm.[2] These bands are often observed to etch white with chemical etchants. White-etching shear bands are commonly observed in quenched and tempered steels. In pearlitic steels, adiabatic shear bands appear as a highly deformed material. The microstructural and mechanical features of these bands are reviewed by Rogers[4] and Mescall and Weiss.[5]

The purpose of this investigation was to determine the effect of metallurgical parameters on the formation of shear bands in 0.18 to 0.20 wt pct carbon steels. Selection of these materials was based on results of previous researchers in the area of adiabatic shear who have extensively studied the medium- and high-carbon steels and who have shown in only a few studies the occurrence of adiabatic shear in low-carbon steels.

MARC. A. MEYERS, Professor of Materials, is with the Department of Applied Mechanics and Engineering Sciences and Center of Excellence for Advanced Materials, University of California–San Diego, La Jolla, CA 92093. CRAIG L. WITTMAN is with Honeywell Defence Systems Division, Hopkins, MN 55343.

Manuscript submitted July 13, 1987.

*This manuscript is dedicated to the memory of John Mescall, who contributed significantly to our understanding of shear bands.

Bedford *et al.*[6] studied a quenched-and-tempered 0.3 pct C steel. Rogers and Shastry[7] determined the hardness of "transformed" bands in quenched-and-tempered AISI 1018 and other steels. They found that the hardness of these bands increased with increasing carbon content. They attributed these very high hardnesses (higher than those obtained by austenitization and quenching of the steels) to an extreme fine grain size and supersaturated carbon in the lattice. More recently, Pintat[8] observed adiabatic shear bands in predeformed low-carbon steel (0.1 pct C). The maximum microhardness was 380 HVH, and the band had the microstructural characteristics of intense plastic deformation ("deformed band").

II. EXPERIMENTAL TECHNIQUES

The formation of adiabatic shear bands was studied using steel targets impacted by cylindrical projectiles at varying velocities. The recovered targets were sectioned and observed. Two low-carbon steels with widely different hardenabilities were chosen as targets: AISI 1018 and 8620. These were impacted by a projectile of AISI W-1 tool steel. Square targets were cut and machined from commercially available stock material to dimensions of 100 × 100 × 12.7 mm. Cylindrical projectiles were cut from 11.1-mm-diameter round bar stock to a length of 13.84 mm. A polypropylene sabot, with dimensions of 16.4 mm in diameter and 15.5 mm in length, was used to carry this projectile through the gun tube. This size was selected from previous researchers' findings that a one-to-one ratio in projectile diameter-to-target thickness is best in such a study.[9] The tail portion of the sabot was flared to a diameter of 16.8 mm, producing a tight seal to the gun tube wall to contain the explosive gases.

The target materials were subjected to diverse treatments in order to provide a wide variety of microstructures. The objectives of these treatments were to provide varieties of yield strengths and work-hardening responses. The microstructural parameters included grain size variations, martensite, tempered martensite, bainite, pearlite, and work-hardening (by preshocking).

Eight diverse treatments were given to the target materials. The AISI 8620 steel has a much greater

hardenability than does the 1018 steel. Therefore, the quench and temper treatments were effective on it.

(1) Shocked: Shock loading was used to work harden the targets without decreasing their thicknesses. A section of the 1018 steel plate was shock loaded with 3 mm of sheet explosive (DETA SHEET*). This was repeated for both faces of the plate, ensuring that the entire cross section was hardened by the shock wave. The DETA SHEET explosive was detonated remotely with a blasting cap, and a 25.4-mm-thick steel anvil was used as a momentum trap to prevent spalling from occurring in the 1018 steel plate. This procedure was chosen to work harden the material because grain sizes and microstructures are essentially retained while the yield strength may rise as much as 20 pct using this procedure. The pressure induced by this process may be estimated using equations for the grazing incidence of explosive detonation on the surface of a plate; it was determined to be 11 GPa.[10]

*DETA SHEET is a trademark of E.I. DuPont de Nemours & Company, Inc., Wilmington, DE.

(2) 1018 Shock-annealed: 1018 shocked material was annealed at 750 °C for 15 minutes, producing a small grain-sized material. This temperature and time condition was determined by optimizing for minimal grain size from different heat-treatment schedules. Grain size reduction has been shown to occur readily in steels shocked and recovery-annealed by previous workers.[11,12]

(3) 1018 Normalized: 1018 targets were normalized by austenitizing at 870 °C for 45 minutes in a commercial nondecarburizing salt bath and air cooling.

(4) 1018 Annealed: 1018 targets were annealed for 72 hours at 870 °C and cooled at a rate of 10 °C per hour, which produced a large grain spheroidized structure.

(5) 8620 Annealed: 8620 target plates were austenitized in vacuum at 870 °C for 6 hours and cooled at a rate of 20 °C per hour, producing a structure with chromium and molybdenum carbides.

(6) 8620 Austempered: 8620 target plates were austenitized at 870 °C for 45 minutes in a commercial nondecarburizing salt bath, quenched into a 500 °C nondecarburizing salt bath for a period of 10 minutes, and then air-cooled. This austempering process produced a bainitic structure.

(7) 8620 Quenched: 8620 target plates were austenitized at 870 °C for 45 minutes in a commercial nondecarburizing salt bath and quenched into an 11 pct iced brine solution, producing a 50 pct martensitic core structure.

(8) 8620 Quenched-and-tempered 200 °C: 8620 steel treated identically as in case 7 was tempered at 200 °C for 1 hour, producing a lightly tempered martensitic core structure.

(9) 8620 Quenched-and-tempered 400 °C: 8620 steel treated identically as in case 7 was tempered at 400 °C for 1 hour, producing a highly tempered martensitic core structure.

Projectiles were austenitized at 800 °C for 10 minutes and quenched into water, with subsequent tempering at 200 °C for 2.5 hours, providing added toughness to maintain shape on impact.

Optical microscopy was performed on all targets prior to impact. Grain sizes were determined for each of the conditions by a mean linear intercept method and with values reported in Table I. Compression specimens were made from each of the material conditions to a standard ASTM, medium length, size ratio. This requires that the diameter-to-length ratio be maintained at 1:3. The specimens were 5.5 mm in diameter and 16.7 mm in length. These specimens were tested in a MTS 810 hydraulic testing system. Tests were conducted at strain rates of 9.7×10^{-4} and 2.5 s^{-1}. Yield strengths, work-hardening, and strain-rate sensitivities were calculated by standard methods. These data are reported in Table I.

For the eight heat-treated conditions and the shocked condition, three separate ballistic impact tests were conducted over a wide range of velocities (450 to 1000 m/s), providing various strain rates on each of the target conditions.

Projectiles were fired from a 0.60 caliber, 1.52-m long, smooth bore gun tube fixed to a Mitchell (V-block) mount (Figure 1(a)). Firing was accomplished by percussion of a mechanical hammer fixed to a 20-mm breach at the end of the gun tube. Targets were positioned 90 deg to the gun tube and at a distance of 35.5 mm with two "C" clamps. Directly behind the target, a fiberboard recovery pack was placed to catch any possible exiting projectile and spall plug (Figure 1(a)). Improved Military Rifle (IMR) 4895 powder of mixed lots was used to accelerate the projectile and sabot. The powder was measured into a 20-mm short case brass cartridge and seated with three tissue wads. The amount of propellant used in each test was dependent on the desired velocity. Impact velocities

Table I. Material Parameters

Material and Condition	Yield Strength (MPa) "Dynamic" (2.5 s^{-1})	Yield Strength (MPa) "Static" (10^{-3} s^{-1})	Grain Size (μm)	Brinell Hardness	Work-Hardening Rate (n)	Strain-Rate Sensitivity (m)
8620 quenched	1,393	1,292	—	426	0.12	0.010
8620 quenched and tempered 200 °C	1,361	1,245	—	404	0.18	0.011
8620 quenched and tempered 400 °C	1,357	1,224	—	352	0.19	0.013
8620 ausquenched	1,057	646	—	290	0.18	0.063
8620 annealed	430	358	27.8	243	0.24	0.024
1018 shocked	717	664	15.5	270	0.15	0.016
1018 shock-annealed	474	358	11.2	240	0.20	0.036
1018 normalized	444	346	18.1	250	0.22	0.032
1018 annealed	350	238	66.2	240	0.26	0.049

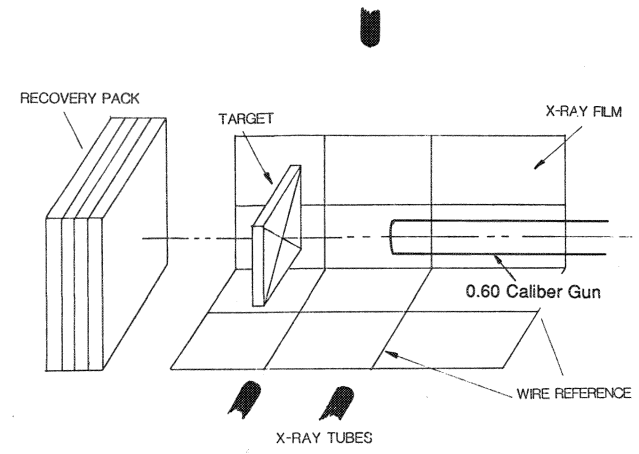

(*a*)

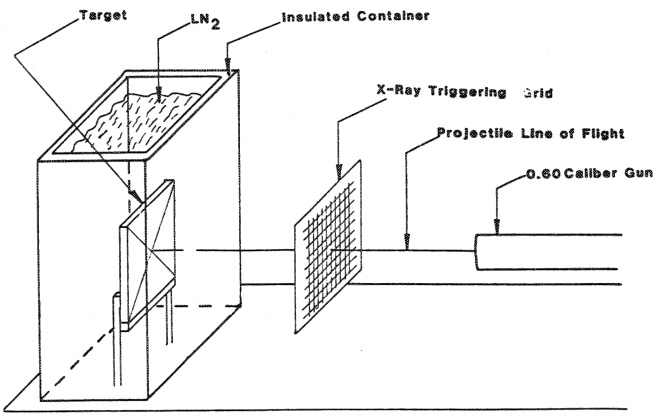

(*b*)

Fig. 1 — Schematic of impact system showing the location of the X-ray tubes and reference wires. (*b*) The low-temperature ballistic test setup, indicating the location of the grid, target, and container to hold the liquid nitrogen.

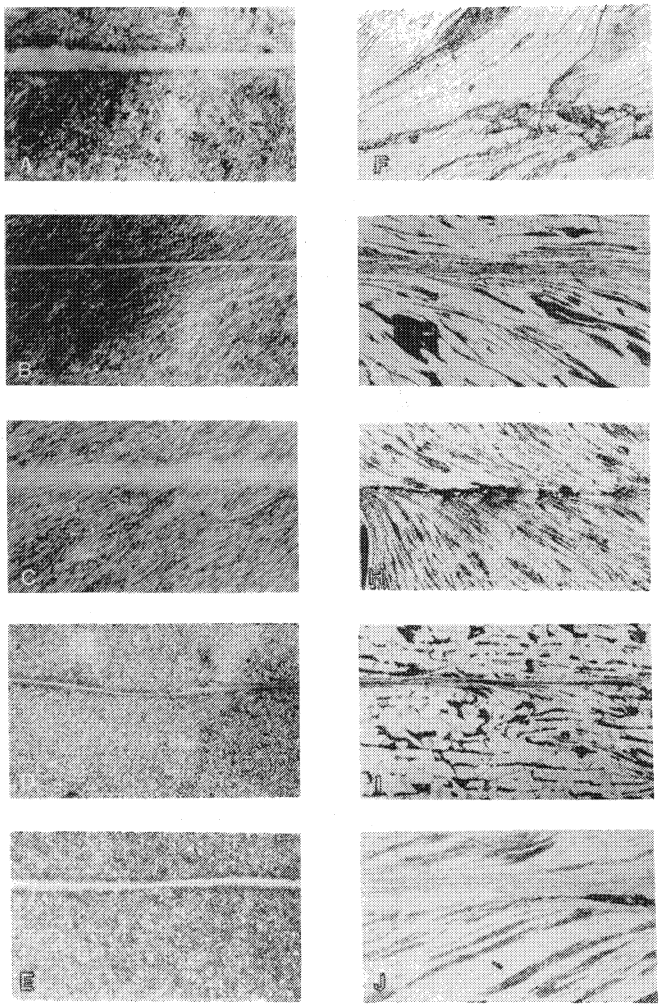

Fig. 2 — Shear bands formed in the various ballistic tests: (*a*) AISI 8620 quenched, (*b*) AISI 8620 quenched and tempered at 200 °C, (*c*) AISI 8620 quenched and tempered at 400 °C, (*d*) AISI 8620 ausquenched, (*e*) W-1 quenched and tempered, (*f*) AISI 8620 annealed, (*g*) AISI 1018 normalized, (*h*) AISI 1018 shocked, (*i*) AISI 1018 shock-annealed, and (*j*) AISI 1018 annealed (strain rate = 10^6 s^{-1} for all conditions).

were measured from flash X-ray images of the projectile in flight. A HEWLETT PACKARD,* three-channel, 105-KV X-ray system was used to perform this. This procedure is described by Grebe *et al.*[13]

*HEWLETT-PACKARD is a trademark of Hewlett-Packard Company, Colorado Springs, CO.

To study the effect of temperature on the propensity to produce shear bands, targets were cooled to liquid nitrogen temperature. This was accomplished by encasing the target into a foam-insulated container filled with liquid nitrogen (Figure 1(b)). This was then allowed to set for 20 minutes, ensuring that the target was completely cooled. The projectile was fired through the wall of the container into the target.

III. RESULTS AND DISCUSSION

After impact, the targets were cross-sectioned both perpendicular and parallel to the rolling direction. A total of 32 ballistic tests were conducted. As a result, shear bands were formed in each of the material conditions (Figure 2). For some of these conditions, higher velocities were required than for other conditions. The density of shear bands was also sharply dependent on the metallurgical condition. The right-hand side shows "deformed" bands; the left-hand side shows "transformed" bands. The latter formed only in the martensitic and bainitic structures.

A. *Penetration and Damage Measurements*

Penetration was measured from the surface of the plate to the deepest portion of the crater (see sketch in Figure 5). When complete plugging had occurred, the penetration was recorded as 12.7 mm, the thickness of the target. Plots of the penetration *vs* impact velocity are presented in Figure 3. A normalized plot was drawn using the kinetic energy of the projectile divided by the dynamic yield stress of the target material as the abscissa (Figure 4). This shows an increase in penetration with increasing normalized kinetic energy (Figure 4). There seems to be a linear relationship between penetration depth and the

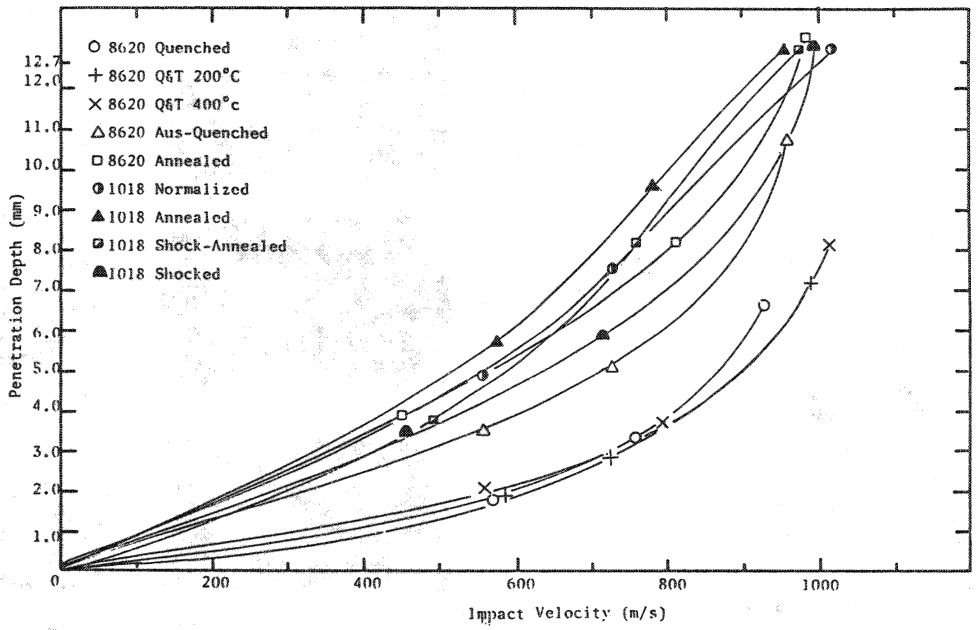

Fig. 3—Plot of impact velocity *vs* measured penetration for all of the room-temperature ballistic tests.

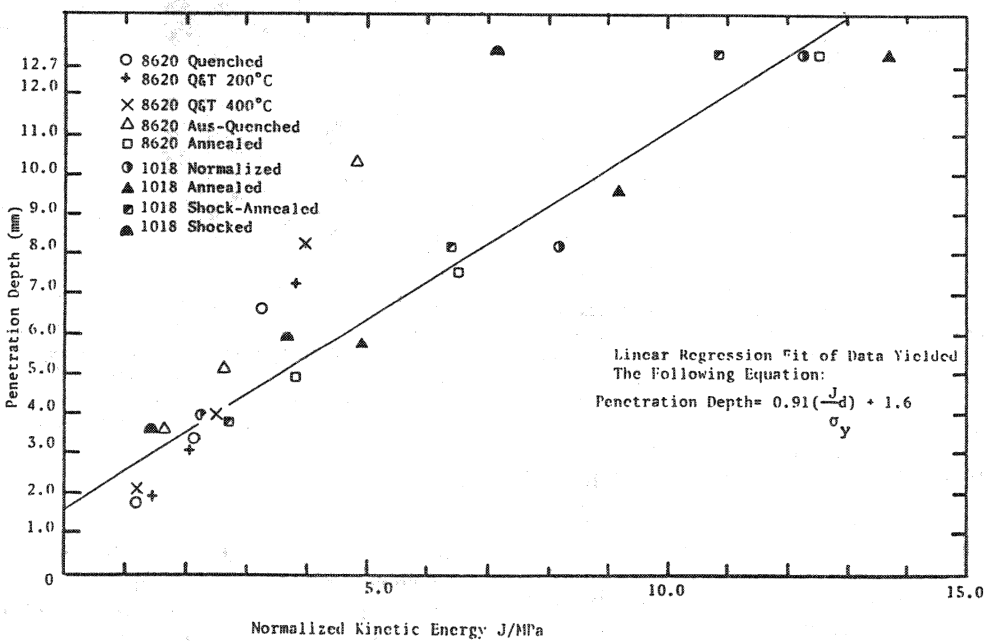

Fig. 4—Plot of normalized kinetic energy *vs* penetration for all of the room-temperature ballistic tests.

normalized kinetic energy. A linear regression provided the following equation:

$$\text{Penetration depth} = 0.91\left[\frac{J}{\sigma_y^d}\right] + 1.6$$

where J is the kinetic energy and σ_y^d is the dynamic yield stress of the target. One can, however, observe a considerable spread in data due, in part, to the important role played by shear bands in the penetration process. The correlation of ballistic data with the kinetic energy of projectiles dates back to de Marre[14] and has been pursued to different levels of complexity by a number of investigators.[15,16]

From the measured impact velocities, the pressure due to the impact was calculated using the impedance matching Hugoniot method.[17]

B. *General Observation*

A generalized schematic of the phenomena observed in impacted targets is shown in Figure 5.[18] Ridges were observed on the surfaces of the crater. These are developed by the deterioration of the projectile as it travels

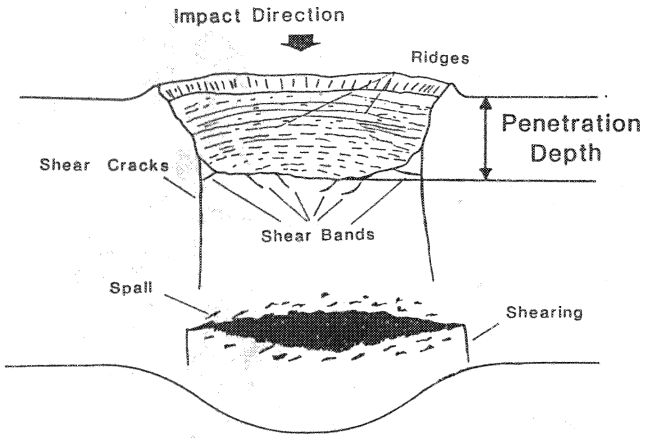

Fig. 5—Generalized schematic of damage expected to be present on impacted targets (adapted from Reference 16).

into the target. Shear cracks are observed at the intersection of the target and the corner of the projectile. These are often parallel to the direction of impact and are preceded by shear bands. Spalling occurred in most samples approximately 2 mm from the rear surface of the target; this is due to the reflection of the shock wave at the free surface. Shear bands were often observed to occur between the voids of the spall and between the outermost edges of the spall and the back surface of the target. Most importantly, shear bands were observed just inside of the impacted region. The region adjoining the impacted surface often etched dark, which is due to a phase transformation to hexagonal close-packed martensite that occurs at pressures above 13 GPa.[19]

The various phenomena identified in the schematic of Figure 5 were present in the sectioned targets. Figure 6 shows the AISI 8620 quenched series impacted at varying velocities. Figure 6(a) indicates the very small amount of deformation which was produced from impact at 570 m/s. A larger amount of deformation is produced from impact at 756 m/s (Figure 6(b)), which shows the dark-etching region near the target projectile interface. Figure 6(c) shows a significant amount of shear banding and spalling, produced from impacting at 926 m/s. Shear bands precede the shear cracks, and near the impact surface, these cracks are intersected by other shear bands. Bands are also observed at the impacted surface.

Comparison of the various amounts and types of damage produced by ballistic impact at a similar penetration depth is shown in Figure 7. Figure 7(a) shows that AISI 8620 quenched and tempered at 200 °C and impacted at 986 m/s exhibits the same damage as the AISI 8620 quenched-impacted at 926 m/s (Figure 6(c)). Spalling is observed, with shearing initiating between the spalled region and the back of the target. Similar shear cracks preceded by shear bands are also observed. An equivalent amount of penetration was produced in AISI 1018 normalized steel impacted at 810 m/s (Figure 7(b)). No shear bands are seen, and the amount of spall separation exceeds the other two conditions. This is indicative of the higher fracture strength and shear band propensity of quenched-and-tempered 8620 as compared

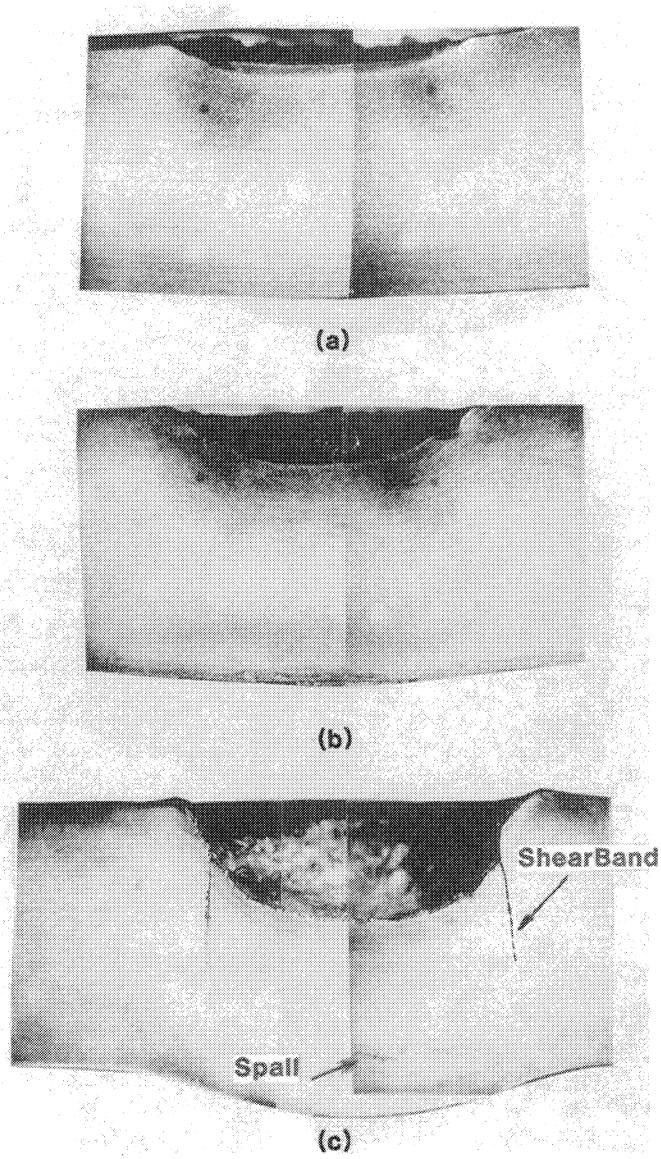

Fig. 6—Cross sections of the AISI 8620 quenched series: (*a*) impacted at 570 m/s, (*b*) impacted at 765 m/s, and (*c*) impacted at 926 m/s. (Shear band highlighted by dashed line.)

to normalized 1018. Shear banding and fracturing of the projectile are also well represented in this micrograph. Figure 7(c) shows AISI 1018 shocked steel impacted at 715 m/s. Shear bands were only found to have occurred between the spall cracks and voids. Previous spalling of the material, due to the preshock loading, is also indicated in this figure by the arrows. Once again, the banding and fracturing of the projectile are well represented in this micrograph.

The back side of the 1018 normalized targets exhibited a spiral pattern (Figure 8). This pattern is a result of trajectories of maximum shear stress removing the oxide surface.[20,21] These travel in a logarithmic spiral pattern through the target plate. If the material exhibits a yield drop (Luders band behavior), plastic deformation will be discontinuous along these surfaces of maximum shear. The spiral patterns shown in Figure 8 represent the intersection of these surfaces with the back surface of the

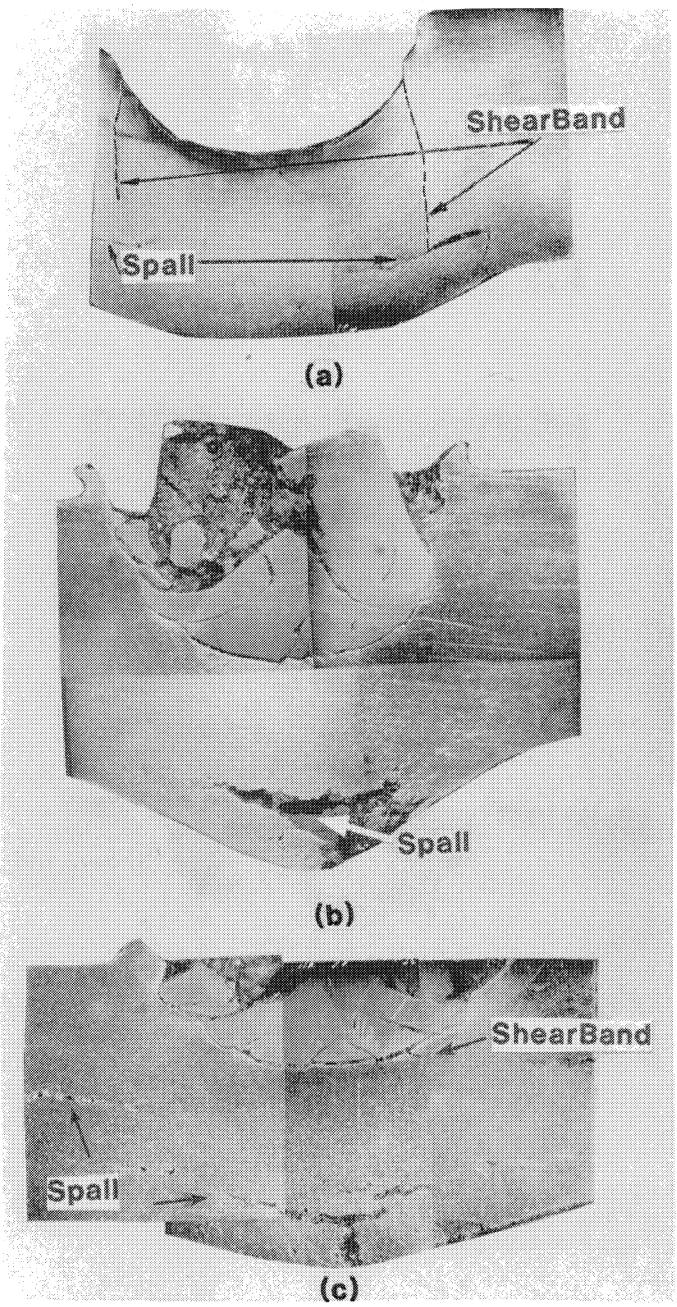

Fig. 7—Cross sections of targets with similar penetration depth: (*a*) AISI 8620 quenched and tempered at 200 °C impacted at 986 m/s (shear band highlighted by dashed line), (*b*) AISI 1018 normalized-impacted at 810 m/s, and (*c*) AISI 1018 shocked and impacted at 715 m/s.

target. They are indicative of nonuniform plastic deformation that could lead to shear instabilities.

The low-temperature ballistic tests did not produce any shear bands at all. No significant plastic deformation was imparted to material, and thus, no shear banding was observed. These targets failed through brittle fracture produced by the reflection of the compressive wave at the back surface (Figure 9). This failure is analogous to failure of unsupported ceramics; the damage characteristics are essentially identical to those observed by Field[22] in glasses and ceramics. The conoid that is produced and the radial cracks are similar, in all respects, to ceramic

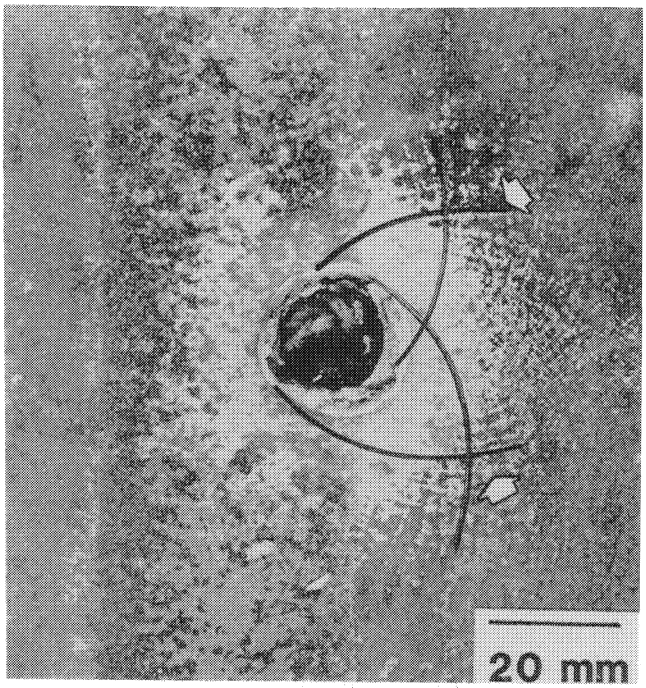

Fig. 8—Macrograph of the removal of oxide by the shear stress spirals.

fracture. Figure 9(b) shows, schematically, the failure mode. The conical fracture is produced by a combination of Hertzian stresses close to impact and tensile reflections, while the radial cracks are produced by bending of the plate. Recent research by Field[22] and Mescall[23] yields similar results. Confined ceramics, in which the tensile stresses due to reflection and bending stresses are eliminated, undergo radically different failure modes under impact. One could speculate that the same holds true for steel. The circular fracturing of the back face of the target is produced by the formation of a spalled conoid. The fracture surface from this spalled region was of a cleavage mode. This was true for all three conditions: shock-annealed 1018, 8620 quenched, and 8620 quenched and tempered at 200 °C.

Plugging of the targets occurred in all of the pearlitic structures exposed to the high-velocity impact range. A micrograph of the spall (Figure 10(a)) indicates that the material failed through ductile tearing in the spall region. The sheared region between the spall and the rear target surface exhibits a brittle fracture surface (Figure 10(b)). The plug surface created by the projectile punching through the entire thickness of the target is presented in Figure 10(c). The plugging possibly produced some local melting, and the failure mechanism in this region was ductile shearing.

C. *Optical Microscopy*

Shear bands observed in the targets varied in location from the expected banding near the impact surface to shear banding between spall cracks. Observation of a "deformed" region at high magnification revealed that the central portion is highly deformed. On the left side of this shear band, a small crack may be observed (Figure 11); the material is 1018 shocked steel. This small

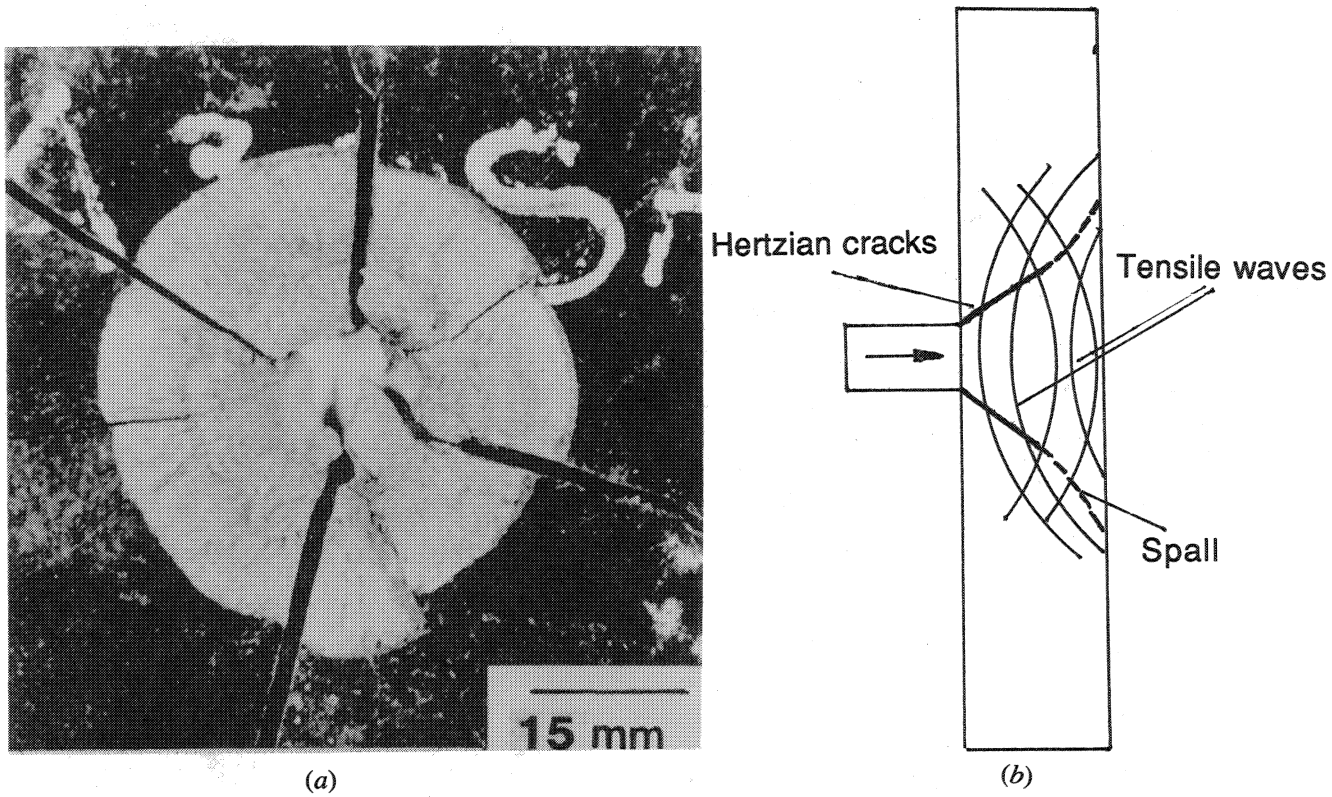

Fig. 9—(*a*) Macrograph showing the spalled region of AISI 1018 shock-annealed target tested at low temperatures (77 K). Note the conical spall removed from the plate. (*b*) Schematic showing formation of conoid by combination of Hertzian contact stresses and tensile reflected stresses.

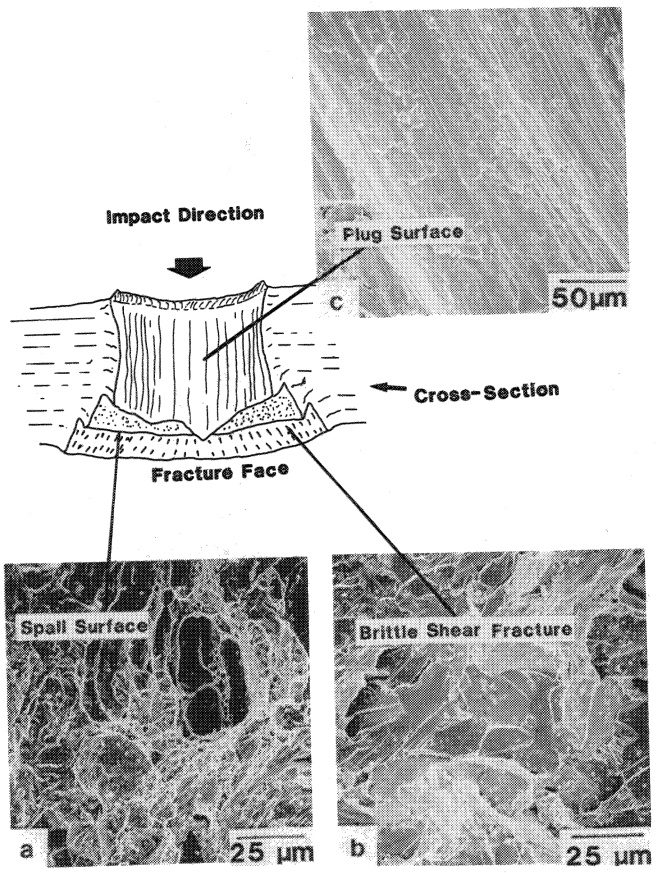

Fig. 10—Scanning electron micrographs of (*a*) spall surface in 1018 shock-impacted at room temperature, (*b*) region between the spall and the rear face of the target, and (*c*) plugging surface.

crack is thought to have been produced in the initial shock loading and not by ballistic impact.

Near the tip of a band in 1018 normalized steel, the differences in displacement may be observed (Figure 12). In the left-hand side, the material is deformed to a much greater degree than the right side. The internal structure of the band may be seen to be very laminar. The darker regions are highly deformed pearlite and the lighter regions deformed ferrite. The occurrence of the brittle pearlite in such a highly deformed state would indicate that a large amount of fracturing of the cementite carbides has taken place.

The band observed (Figure 13) in the 8620 ausquenched steel is illustrative of the processes taking place; both white- and dark-etching regions are found in the shear band. This effect is thought to be due to differences in shear strain. Three smaller, secondary bands are seen to converge toward the principal band. This morphology is consistent with the mechanism for shear band nucleation proposed by Wittman *et al.*[24] The bands nucleate in regions of enhanced plastic deformation, in which the martensitic lamellae align themselves along the flow direction, producing a "geometric" softening. These are incipient bands that develop into full-fledged bands under continued strain. Other bands in the 8620 ausquenched steel were observed near the lip of the impact crater (Figure 14). The cross section is parallel to the rolling direction, hence, the texturing of the matrix material. These bands intersect the texture patterns and indicate the amount of displacement of the shear. It is possible to calculate the shear strain associated with these bands by dividing the displacement (distance between texture marks) by the thickness of the band. These are indicated

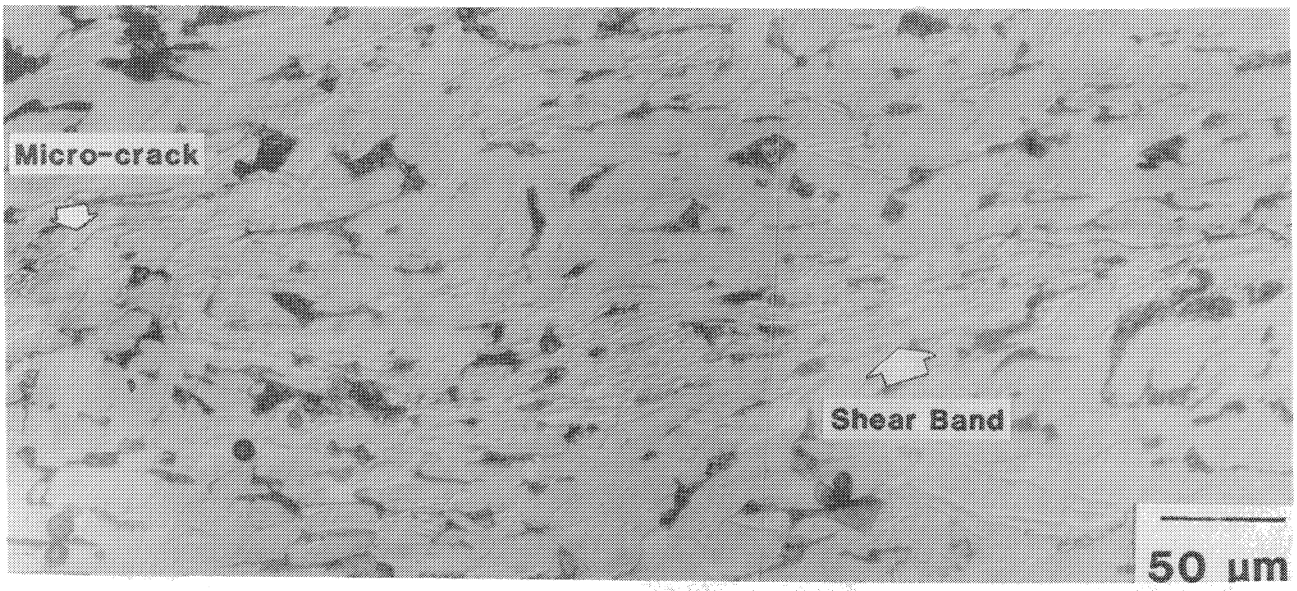

Fig. 11—High magnification of shearing in proximity of a microcrack in AISI 1018 shocked steel.

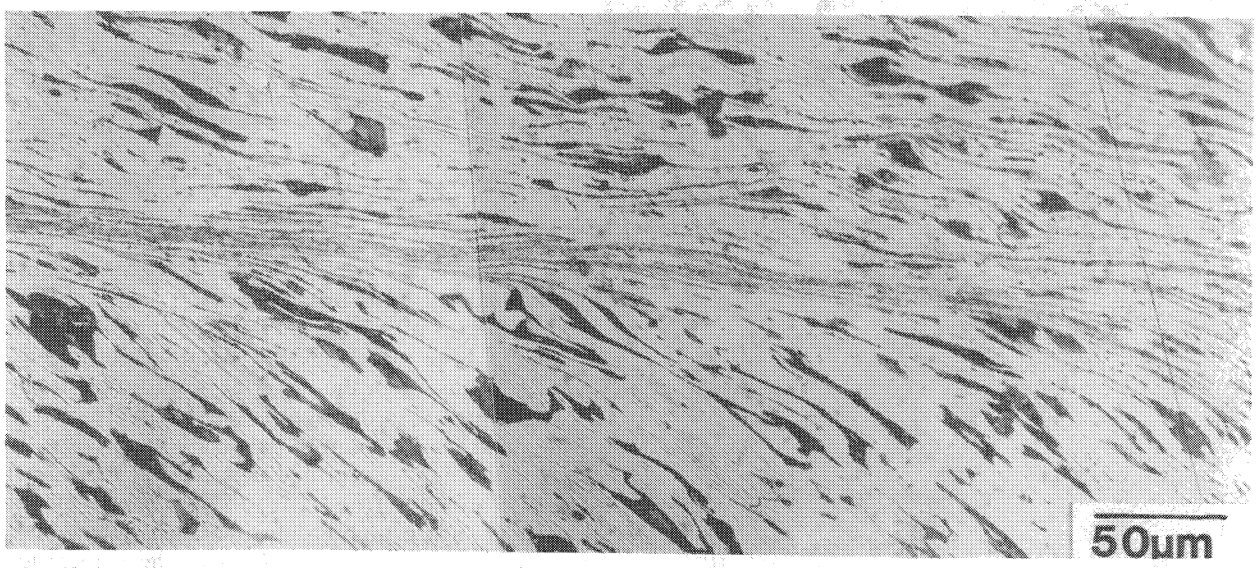

Fig. 12—Tip of band in AISI 1018 normalized steel.

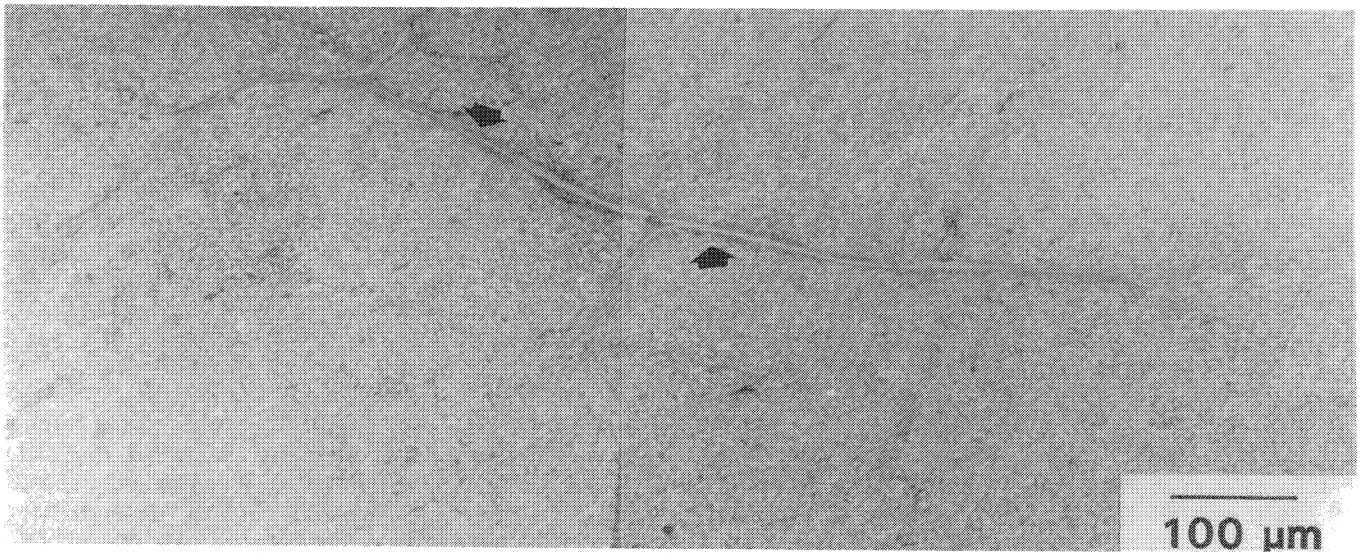

Fig. 13—Shear band in AISI 8620 ausquenched steel. The arrows indicate the regions in which a change from white-etching to dark-etching is observed.

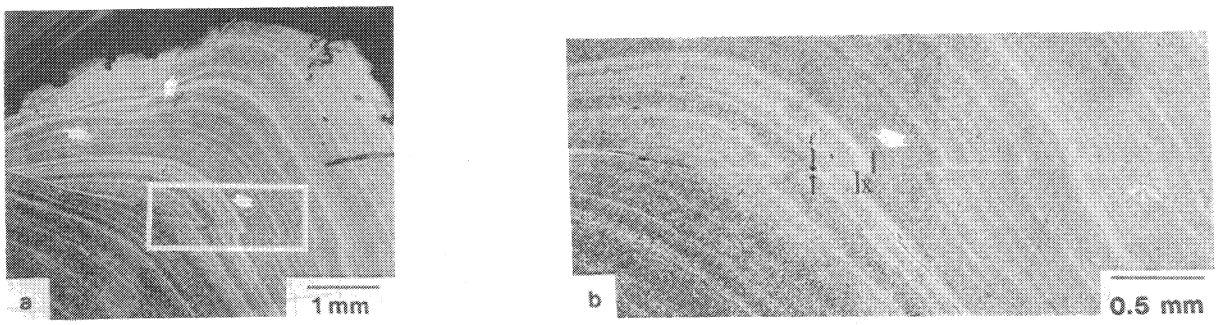

Fig. 14—Shear bands near the lip of a crater in AISI 8620 ausquenched steel: (*a*) note the large displacement as evidenced by the rolling texture; (*b*) "X" indicates the amount of displacement and "ℓ" the width of the band for the shear strain calculation.

by "ℓ" and "X" in Figure 14, respectively. The shear strain is found to be equal to 27.5. This then leads to an approximation of the minimum strain rate by dividing the amount of strain by the duration of impact. The duration of impact may be calculated from the approximation that the kinetic energy decreases linearly, and thus, velocity decreases with the square root of time. For this ballistic test, the duration of impact was 15.5 ms, which results in a minimum strain rate of $1.77 \times 10^6\ s^{-1}$ for this region.

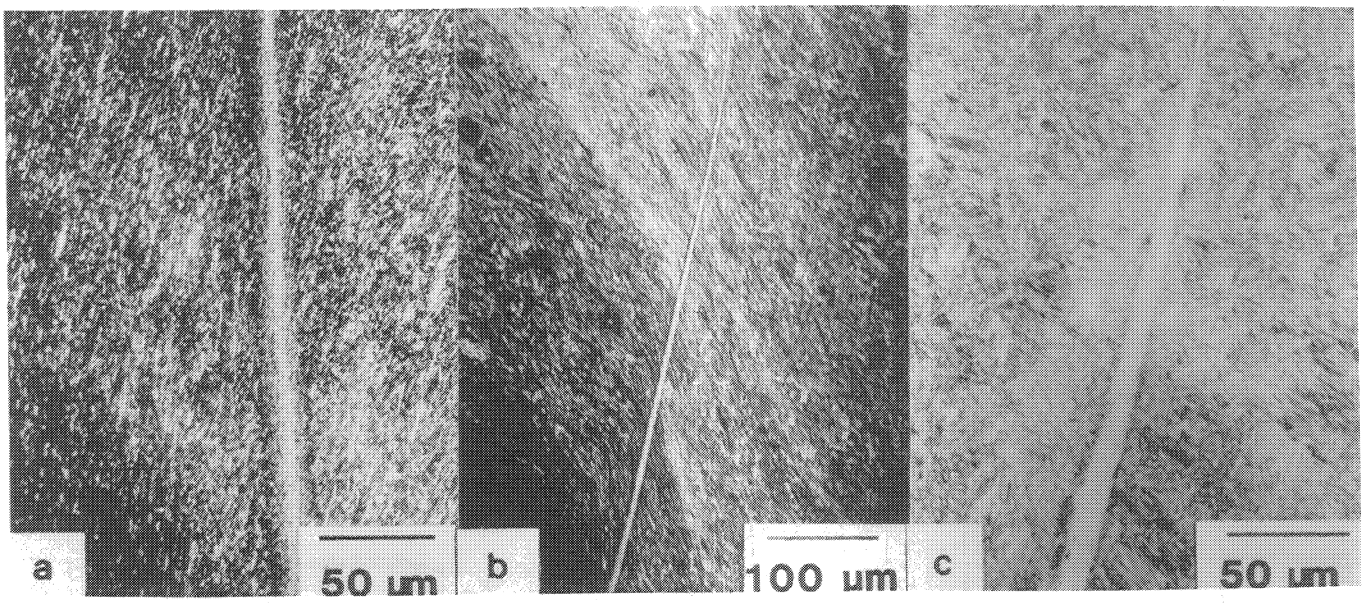

Fig. 15—White-etching shear band in the AISI 8620 (*a*) quenched and tempered at 400 °C, (*b*) quenched and tempered at 200 °C, and (*c*) quenched.

Table II. Shear Band Densities (Total Measured Length in a Cross Section)

Material and Condition	Velocity of Impact (m/s)	Total Length (mm)	
		Parallel	Perpendicular
1018 shocked	715	—	0.35
1018 shock-annealed	926	2.54	—
1018 normalized	807	3.66	—
1018 annealed	780	—	1.31
	953	—	1.40
8620 annealed	978	4.20	—
8620 ausquenched	957	2.00	6.53
8620 quenched	926	7.74	17.07
8620 quenched and tempered 200 °C	986	15.20	14.13
	719	0.66	1.47
	561	—	0.62
8620 quenched and tempered 400 °C	581	—	0.73
	790	—	3.57
	1012	17.34	17.53

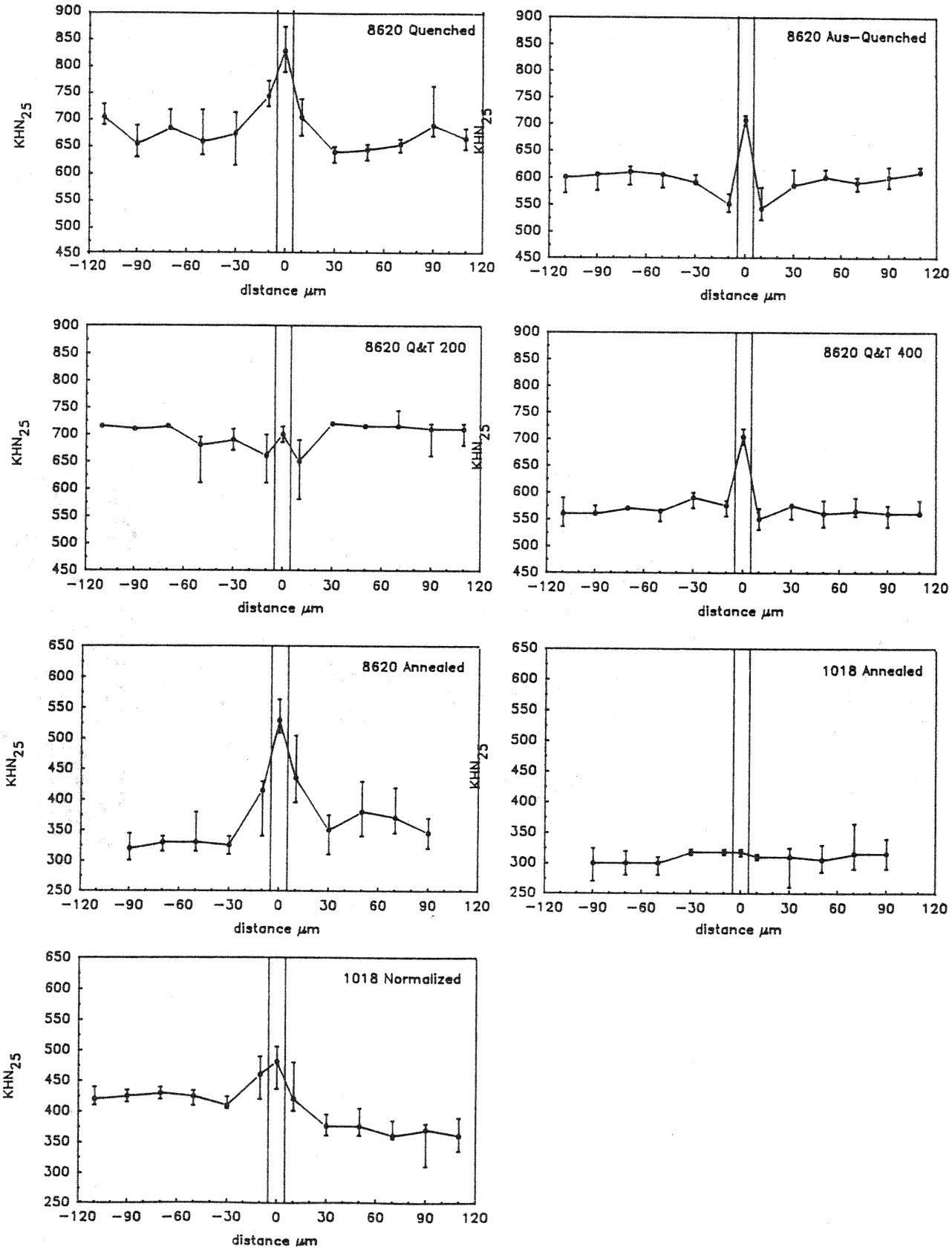

Fig. 16—Microhardness traverses of the material conditions that produced shear bands.

Table III. Critical Microhardness Values for the Shear Bands Observed

Material and Condition	Shear Band			Matrix		
	Average	High	Low	Average	High	Low
1018 shocked	no readings obtainable in shear band					
1018 shock-annealed	no readings obtainable in shear band					
1018 normalized	481	506	438	405	506	325
1018 annealed	318	322	311	299	324	277
8620 annealed	529	564	506	375	470	293
8620 ausquenched	706	715	696	586	617	542
8620 quenched	825	871	784	670	776	607
8620 quenched and tempered 200 °C	700	715	684	649	735	578
8620 quenched and tempered 400 °C	704	721	690	568	607	534

*All values reported were obtained using a Knoop indenter with a load of 25 g for 15 seconds. Averages are results of five readings taken at each location.

Shear bands in the quenched and quenched-and-tempered AISI 8620 steels exhibited the classic white-etching microstructure (Figure 15). The boundary between the band and the matrix is not well defined, and the band path is very straight through the sample, with bifurcation often observed.

Quantitatively, the material most susceptible to shear banding was the 8620 steel quenched and tempered at 400 °C. This was established by measuring the total length of the shear bands in the cross sections made parallel and perpendicular to the rolling direction. In the case of the parallel cross section, only one-half of the cross section could be observed. The measured value was multiplied by 2 to compare for dependencies on rolling direction. These values are reported in Table II and indicate that in the highest velocity range (850 to 1050 m/s), shear bands were found in all of the samples. The results indicate that there may be a greater tendency for shear localization in the planes parallel to the rolling direction in pearlitic steels than for planes perpendicular to it. Conversely, in the quenched steels, more banding existed perpendicular to the rolling direction.

D. *Microhardness*

Microhardness traverses of the shear bands are presented in Figure 16, with the critical data presented in Table III. The hardnesses of the shear bands were found to be independent of impact velocity. Microhardness traverses of bands in the quenched steels produced almost identical results from one impact velocity to another. The results for the quenched 8620 steels indicate that for both the tempered and the ausquenched structures, the hardnesses of the bands were almost identical, while the matrix microstructure hardness varied considerably. This is consistent with earlier results obtained by Rogers and Shastry.[7] They found that the hardness inside transformed bands was a function of carbon content. For a 1018 steel, they found a hardness of ~900 KHN, slightly higher than the hardness obtained in the current study (700 to 800 KHN). The hardnesses of bands in annealed and normalized conditions were much lower and varied considerably. Traverses in the pearlitic structures were more difficult to obtain due to the presence of small microcracks in the bands occurring in the 1018 shocked and 1018 shock-annealed. The indentation was greatly affected by the crack, giving erroneous results. Thus, these traverses are not reported.

It is significant that all but one of the traverses reports an increase in hardness of the band. For the pearlitic steels, this is due to work hardening of the shear localized region. For the white-etching bands, it may be due to work hardening but may also be a result of structural alterations in the shear band.

IV. CONCLUSIONS

The ballistic impact tests showed that white-etching shear bands occur only in the quenched microstructures. If these bands were due to a phase transformation, they would also form in the shocked and ausquenched material that exhibits a reasonably high strength. The penetration resistance of the bainitic microstructure was equivalent to that of the martensitic structures. Hardness traverses of the shear bands in most cases indicated a rise in hardness in the band region. In following the postulation that the white etching of the bands is not necessarily due to a transformation, this hardness rise may be explained as due to a very fine microstructure with supersaturated carbon concentration. The earlier work by Rogers[4] and Rogers and Shastry[7] clearly indicates that the hardness of the "transformed" bands is a direct function of carbon concentration. In a companion paper,[24] it is shown that the structure of the shear band in an AISI 4340 steel (at a strain of 4.9) consists of the same body-centered tetragonal structure as the matrix, with carbides either redissolved or on a much smaller scale; another feature is that the martensite laths are broken down by plastic deformation and replaced by a microcrystalline structure.[8,24] The results obtained by Wittman *et al.*[24] are in accord with the carbide dissolution model proposed by Jones and Sturges.[25] The latter investigators proposed that the white-etching bands form because the dissolution of carbides changes the etching characteristics of the structure. This is consistent with the formation of these white-etching zones exclusively in the quenched and quenched-and-tempered conditions in the present investigation. This type of shear band is classified by Timothy[3] as "transformed." By manipulating the microstructure, as was done, the investigation described herein can produce either "deformed" or "transformed" shear bands, and therefore, the simple thermal diffusivity *vs* critical strain (and strain rate) plots of Timothy are not truly representative of the effects. According to Timothy[3] (Figure 4(b)), the strain rate of

$1.77 \times 10^6\ s^{-1}$ calculated in this investigation would produce "deformed" bands in the 1020 steel. However, 8620 steel, with the same thermal diffusivity, produced "transformed" bands. The formation of shear bands is a complex phenomenon involving strain hardening, thermal softening, and strain-rate hardening, and in which heat transfer plays a major role. The final microstructures observed have to be regarded with caution, and the extent and distribution of strain localization, shear band thickness, and postdeformation microstructures are the result of the interaction among the above parameters. The mechanical aspects of shear band formation have to be considered, and treatments such as Molinari's and Clifton's,[26] Wright's,[27] Wright and Walter's,[28] and Marchand and Duffy's[29] are essential to the overall understanding, because they lead to the prediction of strain localization, shear band thicknesses, and thermal excursion that determine the postdeformation microstructures.

ACKNOWLEDGMENTS

The TERA (Terminal Effects Research and Analysis) staff, and in particular, Mr. D. Collis, who developed and directed all impact experiments, is gratefully acknowledged. The encouragement and financial support provided by Dr. Marx Brook, then Director of the Research and Development Division, New Mexico Tech, is greatly appreciated. The United States Army Research Office provided support for one of us (Marc André Meyers) through Contract No. DAAL03-88-K-0194 in the latter stages of this investigation, and the encouragement provided by Dr. G. Mayer is kindly appreciated. The authors thank Dr. D. Viechnicki (Materials Technology Laboratory) for providing them a copy of Dr. Field's report. The use of the facilities at the Center of Excellence for Advanced Materials at UCSD is gratefully acknowledged.

REFERENCES

1. *Materials Response to Ultra-High Loading Rates*, W. Herrman, ed., NMAB-356, National Materials Advisory Board, National Academy of Sciences, Washington, DC, 1980, pp. 129-42.
2. C. Zener and J.H. Hollomon: *J. Appl. Phys.*, 1944, vol. 15, pp. 22-32.
3. S.P. Timothy: *Acta Metall.*, 1987, vol. 35, pp. 301-06.
4. H.C. Rogers: *Ann. Rev. Mater. Sci.*, 1979, vol. 9, pp. 283-311.
5. *Material Behavior under High Stress and Ultra-High Loading Rates*, J. Mescall and V. Weiss, eds., Plenum Press, New York, NY, 1983.
6. A.J. Bedford, A.L. Wingrove, and K.R.L. Thompson: *J. Austr. Inst. Met.*, 1974, vol. 19, p. 61.
7. H.C. Rogers and C.V. Shastry: in *Shock Waves and High-Strain-Rate Phenomena in Metals*, M.A. Meyers and L.E. Murr, eds., Plenum Press, New York, NY, 1986, p. 285.
8. T. Pintat: in *Impact Loading and Dynamic Behavior of Materials*, C.Y. Chiem, H.-D. Kunze, and L.W. Meyer, eds., DGM Informations-Gesellschaft, Federal Republic of Germany, 1988, p. 737.
9. R.L. Woodward and N.J. Baldwin: *J. Mech. Eng. Sci.*, 1979, vol. 21, pp. 561-68.
10. E.G. Zukas and R.G. McQueen: *Trans. TMS-AIME*, 1961, vol. 221, pp. 412-13.
11. *High Velocity Forming of Metals*, F.W. Wilson, ed., ASTM, Prentice-Hall, Englewood Cliffs, NJ, 1964.
12. W.C. Leslie, E. Hornbogen, and G.E. Dieter: *J. Iron Steel Inst.*, 1962, vol. 177, pp. 622-33.
13. H.A. Grebe, H.-r. Pak, and M.A. Meyers: *Metall. Trans. A*, 1985, vol. 16A, pp. 761-75.
14. J. De Marre: *Memorial de l'Artillerie de Marine*, 1886, vol. 14.
15. M.E. Backman and W. Goldsmith: *Int. J. Eng. Sci.*, 1978, vol. 16, pp. 1-99.
16. T.W. Wright: in *Computational Aspects of Penetration Mechanics*, J. Chandra and J.E. Flaherty, eds., Springer-Verlag, Berlin, 1983, pp. 85-106.
17. *Shock Waves and High Strain-Rate Phenomena in Metals*, M.A. Meyers and L.E. Murr, eds., Plenum Press, New York, NY, 1981, p. 1065.
18. D.A. Shockey, D.R. Curran, and P.S. De Carli: *J. Appl. Phys.*, 1975, vol. 46, pp. 3766-75.
19. R.A. Graham and G.E. Duvall: *Rev. Modern Phys.*, 1977, vol. 49, p. 523.
20. R.E. Rolsten and B.J. Lairmore: *J. Appl. Phys.*, 1976, vol. 47, pp. 983-87.
21. J.S. Rinehart and J. Pearson: *Behavior of Metals under Impulsive Loads*, Dover, NJ, 1965.
22. J. Field: *Investigation of the Impact Performance of Various Glass and Ceramic Systems*, Cavendish Laboratory, Cambridge, MA, U.S. Army Contract DAJA 45-85-C-0021, 1988.
23. J. Mescall: U.S. Army Materials Technology Laboratory, Watertown, MA, private communication, 1988.
24. C. Wittman, M.A. Meyers, and H.-r. Pak: *Metall. Trans. A*, 1990, vol. 21A, pp. 707-16.
25. P.N. Jones and J.L. Sturges: *Inst. Phys. Conf. Ser. No. 7*, Inst. of Phys., 1984, pp. 541-48.
26. A. Molinari and R.J. Clifton: *J. Appl. Mech.*, 1987, vol. 54, p. 806.
27. T.W. Wright: *J. Mech. Phys. Solids*, 1987, vol. 35, pp. 269-82.
28. T.W. Wright and J.W. Walter: *J. Mech. Phys. Solids*, 1987, vol. 35, pp. 701-20.
29. A. Marchand and J. Duffy: *J. Mech. Phys. Solids*, 1988, vol. 36, pp. 251-00.